e-ISSN: 2146 - 9067

International Journal of Automotive Engineering and Technologies

journal homepage:
https://dergipark.org.tr/en/pub/ijaet

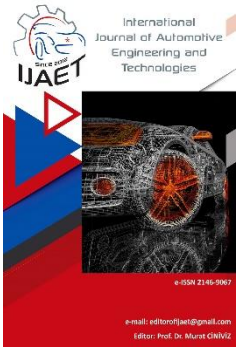

Original Research Article

Generic ground vehicle with variable underbody diffuser: suppressing side leakage

Oğuz Baş[1], Sinan Keyinci[2, *]

[1]Faculty of Engineering, Amasya University, Mechanical Engineering, Amasya, 05000, Türkiye.

[2, *] Faculty of Engineering, Cukurova University Automotive Engineering, Adana, 01380, Türkiye.

ARTICLE INFO

Orcid Numbers
1. 0000-0003-2948-3846
2. 0000-0003-2301-2306

Doi: 10.18245/ijaet.1901680

* Corresponding author
skeiyinci@cu.edu.tr

Received: Mar 03, 2026
Accepted: Jun 02, 2026
Published: 22 Jun 2026

Published by Editorial Board Members of IJAET

To cite this paper: Baş, O., Keyinci, S., Generic ground vehicle with variable underbody diffuser: suppressing side leakage, International Journal of Automotive Engineering and Technologies., 15 (2), 91 – 101. 2026.
http://dx.doi.org/10.18245/ijaet.1901680

ABSTRACT

The Ahmed body is one of the most widely used generic models in automotive aerodynamics. Rear underbody diffusers are known to improve aerodynamic performance by enhancing pressure recovery. However, detailed flow analysis indicates that localized low-pressure regions and lateral vortex structures can limit the effectiveness of a fixed diffuser configuration. In this study, the flow behavior of a 35° Ahmed body equipped with an optimized underbody diffuser is investigated numerically. The analysis focuses on the detailed wake topology and pressure evolution along the diffuser surface to better understand the governing flow mechanisms. Flow visualizations show that side leakage and vortex cores developing near the lateral edges intrude into the diffuser channel and disturb the intended expansion process. To address this limitation, a variable-angle diffuser configuration is proposed and parametrically evaluated. The geometry is adjusted to control the lateral vortex interaction and stabilize the underbody expansion. The variable diffuser reduces side leakage intensity and improves wake alignment. Compared to the fixed diffuser configuration, an additional drag reduction of 51 drag counts is achieved. The results highlight that diffuser performance depends not only on the expansion angle but also on its interaction with lateral flow patterns developing near the underbody and wake regions.

Keywords: Ahmed body, underbody diffuser, side leakage, wake structure, aerodynamic drag reduction.

1. Introduction

Aerodynamic drag represents a significant part of the total resistance acting on road vehicles and directly affects fuel consumption and driving range. While global body shape optimization has long been a primary focus in vehicle design, increasing attention has been directed toward localized flow structures that strongly affect rear pressure distribution [1,2]. The underbody region influences how the flow is directed toward the wake. Changes in diffuser geometry can modify pressure recovery in this area [3]. The interaction between accelerated underbody flow, ground proximity effects, and lateral vortex structures

can modify the stability and orientation of the wake, especially for bluff-body configurations operating close to the ground [4]. For this reason, understanding and managing the three-dimensional flow near the diffuser and side edges remains an important topic in ground vehicle aerodynamics.

Simplified ground vehicle models are used to study wake dynamics and underbody flow without the geometric details of production vehicles. Among these benchmark geometries, the Ahmed body is one of the most widely studied configurations. It represents characteristic aerodynamic features such as clear separation points, base pressure deficit, and stable wake structures for different rear slant angles [5–7]. Experimental and numerical studies have shown that, even for the same nominal geometry, modeling approaches and boundary conditions can alter the wake topology and the resulting aerodynamic coefficients [8,9].

In recent years, research has expanded beyond rear slant effects toward the near-ground and lateral regions. Wheel and wheelhouse details have been shown to reorganize the vortex system feeding the wake and to modify pressure recovery at the base. For example, wheelhouse shape variations were shown to affect the near-wake structure and aerodynamic forces even for the 35° slant configuration [10], and different wheel configurations were reported to redistribute drag contributions between wheels and bodywork [11]. Underbody aerodynamic performance depends on diffuser geometry as well as the evolution of lateral vortex structures forming near the side edges and wheelhouse regions. Vortices generated in these areas can interact directly with the expanding flow inside the diffuser channel and modify the intended pressure recovery process. Moreover, studies investigating the Ahmed body under crosswind conditions have shown that lateral flow components significantly reorganize the wake structure and alter both drag and lift behavior [12]. Even moderate crossflow can shift vortex core positions and modify base pressure distribution. Such vortex displacement demonstrates that lateral momentum can penetrate toward the base region and interfere with diffuser expansion. Controlling side-induced vortex penetration in diffuser-equipped configurations therefore becomes a primary design consideration. Accordingly, lateral leakage mechanisms within diffuser-equipped configurations deserve closer and more systematic investigation.

Rear underbody diffusers are commonly studied as passive flow control devices in simplified ground vehicle configurations. Several numerical and experimental studies indicate that diffuser inclination, expansion ratio, and ground clearance strongly influence pressure recovery and lift–drag characteristics of the Ahmed body [13–16]. Buscariolo et al. [13] demonstrated that diffuser angle optimization can significantly modify base pressure levels in simplified Ahmed configurations, while Huminic and Huminic [15] showed that curvature and diffuser slope affect separation onset inside the expansion channel. Guerrero et al. [14] reported that rear underbody diffusers can alter wake topology and improve aerodynamic forces in road car models. More recent computational analyses also confirmed that diffuser geometry changes shift the balance between pressure drag reduction and lift generation in steady-state simulations [16,17]. In addition to geometric modifications, experimental studies on realistic vehicle models have shown that the wake structure is extremely sensitive to the underbody flow momentum. Wind tunnel investigations revealed the presence of two distinct wake states associated with different base pressure gradients and drag levels, and a controlled reduction of underbody velocity was reported to induce drag variations of nearly 10% [18]. Other studies have also examined how modifications to the diffuser's external geometry influence underbody flow behavior. Porcar et al. [19] investigated the effect of adding vertical airfoil endplates to a simplified diffuser model and found that such endplates can significantly alter flow patterns and pressure recovery by changing vortex behavior near the diffuser exit, which in turn impacts downforce and drag performance.

Although these studies clarify the influence of diffuser geometry on global aerodynamic behavior, the detailed interaction between lateral vortex structures and the diffuser

expansion channel remains insufficiently explored. Most parametric investigations still rely on fixed-angle diffuser configurations evaluated under nominal flow alignment. Even when wheel effects or boundary condition variations are considered, the discussion generally remains limited to global aerodynamic coefficients rather than localized three-dimensional interactions [10,20,21]. Studies addressing wheelhouse geometry and lateral flow development revealed that vortex systems generated near the side edges and wheel regions can reorganize the near-wake structure and redistribute drag contributions. However, their direct coupling with the internal diffuser expansion process is rarely treated as an explicit design parameter. Flow visualizations of diffuser-equipped Ahmed configurations frequently display low-pressure pockets and asymmetric structures along the underbody, suggesting that diffuser performance is influenced by side-induced vortex intrusion in addition to geometric slopes.

To address this limitation, the present study introduces a variable-angle underbody diffuser designed specifically to control lateral vortex penetration into the expansion channel. Unlike conventional fixed-slope designs, the expansion angle is adjusted parametrically to control vortex positioning and reduce side-induced penetration into the diffuser channel. The novelty of the present work lies in treating the diffuser angle not only as a geometric parameter for pressure recovery, but also as a tool for managing lateral vortex interaction. The configuration is evaluated using RANS simulations in Ansys Fluent, and its aerodynamic performance is assessed through drag coefficient, pressure distribution, and mass flow exchange analyses. The results confirm that suppressing lateral vortex penetration yields an additional drag reduction of 51 drag counts together with a clear decrease side leakage intensity.

2. Materials and Methods

2.1. Geometry description

The numerical model used in this study is based on the 35° Ahmed body configuration, which is widely adopted as a benchmark geometry for ground vehicle aerodynamics. The main geometric parameters of the model are illustrated in Figure 1. The total body length is 1044 mm, the height is 288 mm, and the width is 289 mm. The rear slant angle is fixed at 35°, corresponding to the commonly studied low-drag configuration. The ground clearance is set to 50 mm, consistent with previous experimental and numerical studies.

To assess the mass flow under and upper sides of the body, two measurement planes were created during the geometry creation process. The selected plane locations are illustrated in Figure 1. The under plane was created at x=-626.4mm, y ∈ [0mm - 50mm] and z ∈ [-194.5mm - 194.5mm] while upper planes were at x=-626.4mm, y ∈ [338mm- 388mm] and z ∈ [-194.5mm - 194.5mm].

The underbody section includes a diffuser region starting from the rear lower edge of the model. In the reference configuration, the diffuser angle is fixed, and the expansion length is 626.4 mm. The diffuser geometry was optimized to improve aerodynamic performance. Moreover, detailed flow analysis revealed a non-uniform pressure distribution and noticeable vortex activity near the side edges of the diffuser. For the proposed design, the diffuser angle is treated as a variable parameter while preserving the main body geometry.

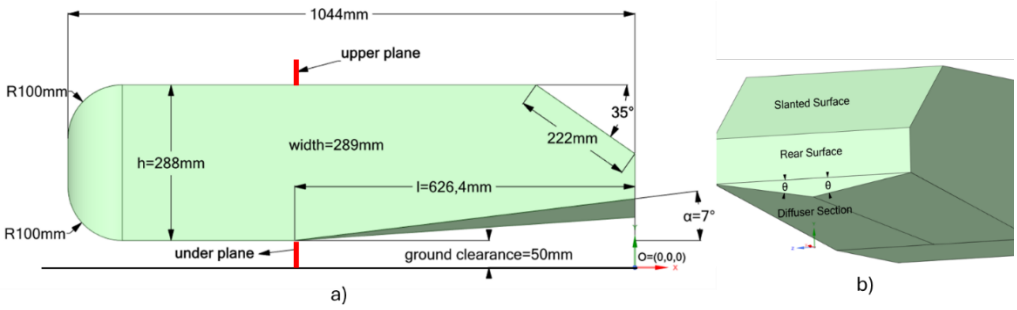

Figure 1. Geometry and main dimensions of the 35° Ahmed body with underbody diffuser: a)side view b)back view.

2.2. Computational domain and boundary conditions

The computational domain was defined with sufficient spatial extent to allow realistic wake development and to minimize confinement effects on the flow field. Particular attention was given to maintaining an appropriate distance between the vehicle model and the domain boundaries in order to avoid artificial pressure gradients and velocity distortions. The domain dimensions were set to 15L in the streamwise direction, 3L in the lateral direction, and 2L in the vertical direction, where L represents the vehicle length. The vehicle cross-sectional area is 112032 mm², resulting in a blockage ratio of 2.386%, which remains within acceptable limits for external aerodynamic analyses. The flow was modeled as fully three-dimensional, steady, and incompressible. RANS equations were solved to capture the mean flow behavior associated with diffuser expansion and lateral vortex interaction.

A uniform velocity inlet of 40 m/s was prescribed at the upstream boundary. At the outlet, a pressure outlet condition with zero-gauge pressure was applied. The vehicle body and ground surface were treated as stationary no-slip walls. The top and lateral boundaries were defined as symmetry surfaces to approximate free-stream conditions and to minimize wall-induced interference. The main properties of the computational domain and boundary conditions are summarized in Table 1. In addition to the evaluation of global aerodynamic coefficients, mass flow rates were calculated across selected cross-sectional planes located near the diffuser outlet and lateral regions.

2.3. Grid Generation and Mesh Refinement Strategy

The numerical grid was generated using a poly-hexcore meshing strategy to achieve a balance between computational efficiency and spatial resolution. Special attention was given to resolving the near-wall regions of the vehicle body and the diffuser section, where strong velocity gradients and vortex structures are expected. The computational domain was divided into three refinement regions to control element size distribution more effectively and to preserve mesh quality within the wake development zone. Local refinement was concentrated around the underbody and rear regions to capture the flow expansion inside the diffuser channel with sufficient accuracy.

Table 1. Properties of the computational domain and boundary conditions

Boundary Conditions		**Computational Domain**	
Inlet	Velocity Inlet (40 m/s)	**Flow Field**	quasi-3D, steady, and incompressible flow
Outlet	Pressure outlet (0 Pa)	**Length X width X height**	15L X 3L X 2L
Body surface and ground	Stationary wall (No-slip)	**Vehicle cross-sectional area**	112032 mm^2
Top and sidewalls	Free slip (symmetry)	**Blockage ratio**	2.386%

Table 2. The meshing strategy of this numerical study

	Mesh 1	**Mesh 2**	**Mesh 3**	**Mesh 4**
Element size of the Region I (mm)	20	10	6	5
Element size of Region II (mm)	40	20	16	12
Global element size (Region III) (mm)	256	128	128	128
First prism layer height (mm)	0.04	0.02	0.01	0.01
Number of prism layer	25	25	25	25
Growth rate	1.2	1.2	1.2	1.2
Volume mesh type	Poly-hexcore	Poly-hexcore	Poly-hexcore	Poly-hexcore
Total mesh count (x10^6)	1.2	1.98	3.98	5.96
Drag Coefficient (C_D)	0.3032	0.2708	0.2668	0.2655

Table 3. Comparison of force coefficients of CFD setups with the experimental data

Parameter	Experimental [5]	Experimental [9]	Experimental [20]	Numerical (Current Study)
Re_L	4.29×10^6	2.78×10^6	2.78×10^6	2.78×10^6
C_D	0.2580	0.2790	0.2580	0.2655
C_L	n.a.	0.0040	-0.0300	-0.0050

Prism layers were generated along all solid surfaces to resolve the boundary layer development accurately. A total of 25 prism layers were applied with a growth rate of 1.2 to ensure gradual transition from the wall to the core region. The first prism layer height was defined according to the targeted near-wall resolution and was progressively refined across different mesh levels. The element size distributions for Region I (near-body zone), Region II (intermediate refinement zone), and Region III (outer domain) are summarized in Table 2. Four mesh configurations were constructed to evaluate sensitivity to grid resolution. The total cell count ranged from 1.2 million to 5.96 million elements. Mesh refinement was particularly intensified in the diffuser and wake regions, where strong shear layers and vortex cores are present. This refinement strategy allowed improved resolution of underbody expansion and lateral flow interaction without excessive increase in computational cost. The final selection of the grid level is Mesh 3 since following level varies approximately 1.3 drag counts only. Therefore, Mesh 3 was selected for all subsequent simulations to achieve an optimal balance between numerical accuracy and computational cost, as further grid refinement yielded negligible performance changes.

2.4 Turbulence model and model validation

To accurately resolve the complex three-dimensional flow separation and vortex interactions over the vehicle rear, the Shear Stress Transport (SST) k-ω turbulence model was employed for all numerical simulations. This model effectively combines the robustness of the standard k-ω formulation in the near-wall region with the freestream independence of the k-ε model in the far-field. Regarding the wall treatment approach, a low-Reynolds-number near-wall modeling strategy was adopted instead of standard empirical wall functions. To fully resolve the viscous sublayer, the computational mesh was heavily refined near the solid vehicle surfaces, maintaining a maximum non-dimensional wall distance y^+ of approximately 1. This rigorous wall-bounding approach ensures high fidelity in predicting skin friction and localized flow detachment along the diffuser boundaries.

The numerical setup was validated by comparing the aerodynamic force coefficients of the baseline 35° Ahmed body configuration with experimental data reported in the literature. The comparison is presented in Table 3. The Reynolds number based on vehicle length in the present study is 2.78×10^6, which corresponds to the experimental conditions reported in [9,21]. The computed drag coefficient is 0.2655, while experimental values at similar Reynolds numbers vary between 0.2580 and 0.2790 depending on test setup.

For the lift coefficient, the predicted value is −0.0050. Experimental data available at similar Reynolds numbers indicate near-zero lift behavior for the 35° configuration, with reported values of 0.0040 and −0.0300. The numerical result falls within this range. The variations in the drag coefficient (C_D) compared to the experimental measurements available in the literature can be primarily attributed to conventional numerical error sources, including the physical modeling limitations of the turbulence closure, spatial discretization errors, iterative convergence criteria, and round-off precision may also account for these variances. Furthermore, it is worth noting that experimental measurements inherently carry a certain degree of uncertainty and potential systematic errors.

The agreement between numerical predictions and the experimental data confirms that the computational approach is suitable for comparative aerodynamic analysis of the diffuser configurations examined in this study.

3. Results and Discussion

The aerodynamic behavior of the baseline and modified configurations was evaluated through both qualitative flow visualization and quantitative force analysis. Comparisons were conducted between the base model, the fixed-angle diffuser configuration, and the proposed variable-angle diffuser design. The analysis concentrates on the wake structure, pressure distribution within the underbody region, and the interaction between lateral vortex systems and the diffuser channel. In addition to the drag and lift coefficients, mass flow transfer between the underbody and side regions was quantified to clarify the mechanism responsible for side leakage development.

The velocity contours on the symmetry plane for the three configurations are presented in Figure 2. In the base model, the flow separates near the rear slant and forms a broad low-velocity wake region extending downstream. The underbody's flow remains relatively uniform and does not exhibit significant acceleration before entering the wake. When the fixed diffuser is introduced, a noticeable increase in underbody velocity is observed. The flow accelerates along the diffuser surface and exits with higher momentum, resulting in a narrower wake structure compared to the base case. In the variable diffuser configuration, the acceleration along the underbody is distributed over a longer streamwise distance, and the high-velocity region beneath the vehicle extends further downstream with improved alignment toward the wake centerline.

The lateral velocity component on the side plane is illustrated in Figure 3, providing clearer insight into the side leakage mechanism. In the base configuration, the lateral velocity magnitude remains relatively weak beneath the vehicle, and the wake structure is predominantly aligned with the streamwise direction. With the addition of the fixed diffuser, however, a pronounced lateral velocity region develops near the diffuser exit. A concentrated band of negative lateral velocity forms along the lower side edge, indicating intensified crossflow from the underbody toward the wake. This behavior demonstrates that the accelerated underbody jet interacts with lateral vortex structures and enhances cross-channel momentum transfer. In contrast, the variable diffuser configuration exhibits a more contained lateral velocity distribution. Although underbody acceleration is still present, the magnitude and spatial extent of the negative lateral velocity beneath the diffuser are visibly reduced compared to the fixed diffuser case.

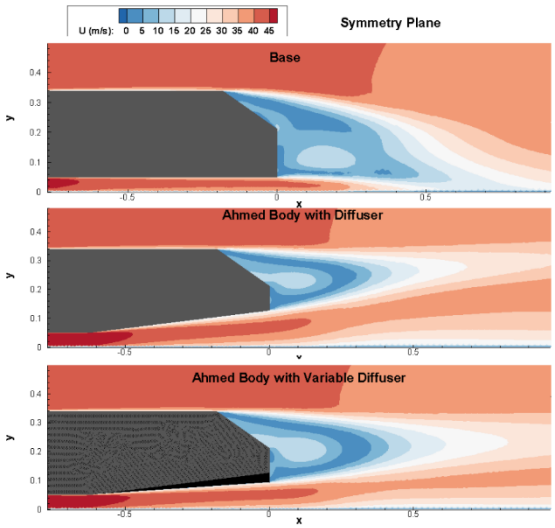

Figure 2. Symmetry plane velocity contours.

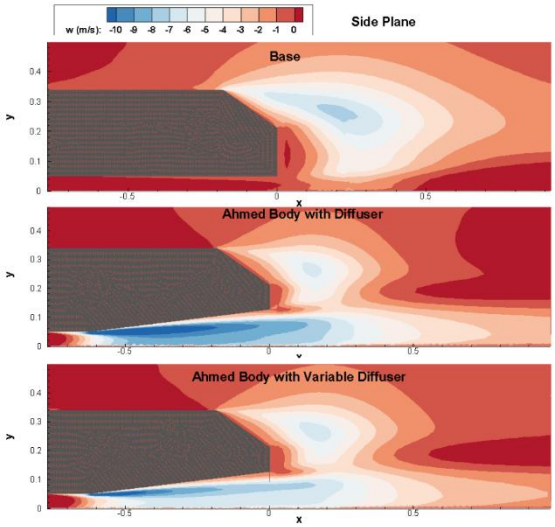

Figure 3. Side plane velocity contours.

Streamline topology offers a direct view of how the diffuser designs reshape the near-wake recirculation. As seen in Figure 4, the baseline configuration is dominated by a single, coherent recirculation structure downstream of the rear slant, with the separated shear layer forming a stable vortex core in the upper wake region. Introducing the fixed-angle diffuser fundamentally changes this topology. The accelerated underbody flow leaves the diffuser with higher momentum and

creates a secondary recirculation region near the outlet. An upper and lower vortex form, and the recirculation zone extends downstream. In the variable angle diffuser case, the wake pattern remains similar, but the lower recirculation region is smaller and more stable than in the fixed angle configuration.

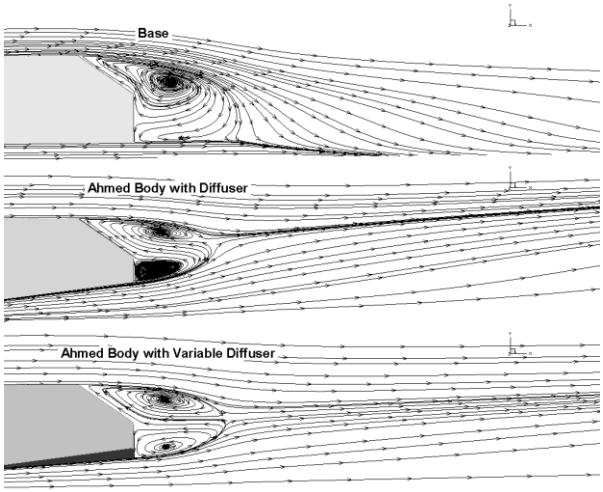

Figure 4. Streamline patterns on the symmetry plane.

The variation of aerodynamic coefficients with diffuser angle is shown in Figure 5. Both drag and lift change noticeably with the diffuser angle. The lowest values are obtained when the angle is around ten degrees, indicating a favorable expansion range. As the diffuser angle is reduced from higher values toward this region, the drag coefficient decreases. When the angle is reduced further beyond this point, drag begins to increase again. The fixed diffuser configuration reduces drag compared to the base case, and the variable-angle configuration provides an additional improvement. A similar tendency is observed in the lift coefficient, where moderate diffuser angles result in more favorable aerodynamic behavior, consistent with improved underbody flow development and pressure recovery beneath the vehicle.

To clarify the change in aerodynamic forces, mass flow rates through the underbody and upper regions were evaluated. In the base model, the underbody mass flow is 0.9828 kg/s. This value increases to 1.1606 kg/s with the fixed diffuser and remains high at 1.1186 kg/s for the variable diffuser configuration. The upper-region mass flow stays almost constant for all cases, around 0.97 kg/s. This shows that the improvement in drag is mainly related to the modification of the underbody flow. The diffuser increases the flow passing under the vehicle and changes the momentum distribution near the base region. In the variable configuration, the underbody mass flow is slightly lower than in the fixed diffuser case, which indicates a smoother expansion process and reduced interaction between the underbody jet and the lateral vortex structures.

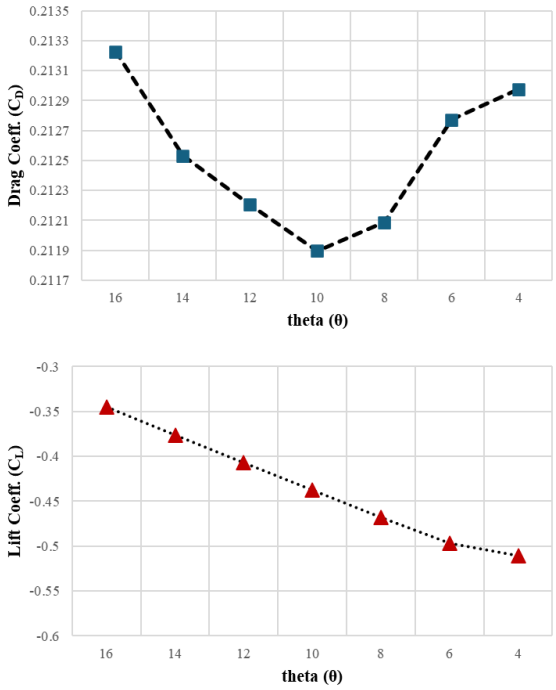

Figure 5. Influence of diffuser expansion angle on aerodynamic force coefficients

A more detailed examination of the vortex interaction is provided in Figure 6, where the symmetry-plane streamlines are marked with representative vortex core locations. In the fixed diffuser configuration, the primary recirculation core is positioned closer to the diffuser exit, while secondary structures develop near the lower region of the wake. The streamline topology reveals a closer spatial interaction between the expanding underbody jet and the lateral vortex structures. The side-originating vortex core is located nearer to the diffuser exit, promoting increased cross-stream momentum transfer into the wake region. For the variable diffuser case, the primary vortex core shifts slightly downstream and away from the diffuser surface. The lateral penetration into the diffuser flow is therefore limited, and the intensity of the side leakage decreases. Under these conditions, the underbody jet connects with the wake more directly, supporting the reduction in drag

observed in the force analysis.

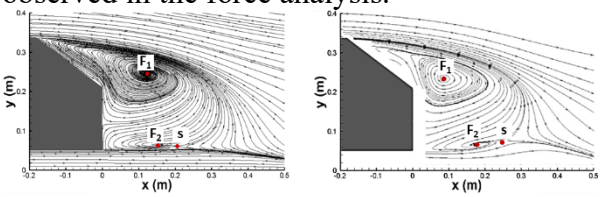

Figure 6. Comparison of vortex core locations and wake structure on the symmetry plane.

The pressure distributions shown in Figure 7 further explain the differences observed in aerodynamic performance. In the base configuration, a broad low-pressure region forms behind the slanted surface, while the underbody pressure remains relatively moderate. The wake is characterized by a wide pressure deficit extending downstream. With the fixed diffuser, a stronger pressure drop develops beneath the vehicle due to accelerated underbody flow. However, localized low-pressure pockets appear near the side edges of the diffuser exit. These regions correspond to the intrusion of lateral vortex structures into the expansion channel. Although the diffuser increases base pressure recovery compared to the base model, the side-induced disturbances limit the effectiveness of the expansion process. In the variable diffuser configuration, the pressure distribution beneath the vehicle becomes more uniform. The intense low-pressure pockets near the lateral edges are reduced, and the base pressure region appears more stable and symmetric.

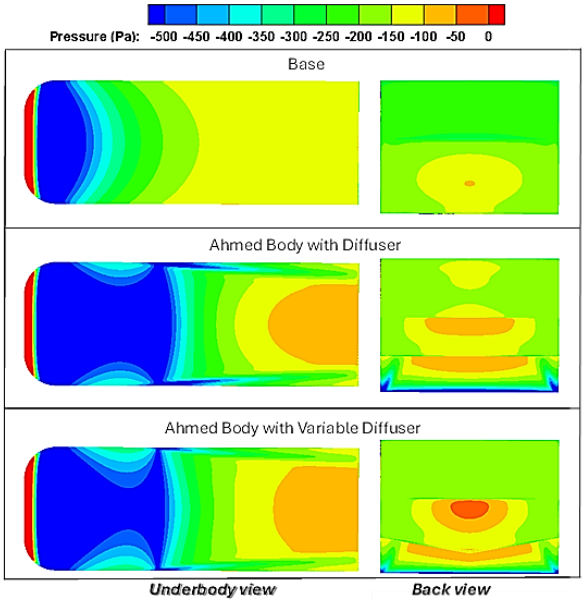

Figure 7. Pressure contours for the base, fixed diffuser, and variable diffuser configurations.

The aerodynamic force coefficients of the three configurations are summarized in Table 4. The introduction of the fixed diffuser reduces the drag coefficient from 0.2655 to 0.2170, corresponding to a reduction of 485 drag counts. The variable diffuser configuration further decreases the drag coefficient to 0.2119, resulting in a total reduction of 536 drag counts compared to the base model. In terms of lift behavior, the base configuration exhibits nearly neutral lift. Both diffuser configurations generate negative lift due to increased underbody acceleration and the associated pressure reduction beneath the vehicle. The fixed diffuser produces a lift coefficient of −0.5045, while the variable diffuser results in a slightly smaller magnitude of −0.4374. Although the variable diffuser generates less downforce than the fixed configuration, it provides improved drag performance, leading to a more favorable overall aerodynamic balance.

The compiled aerodynamic trends and underbody flow behaviors observed in this study demonstrate strong qualitative and quantitative correlations with several prominent investigations in literature. The fundamental mechanics of underbody pressure recovery and wake alterations found here align with the insights of Huminic and Huminic, who highlighted the capability of rear diffusers to modify near-wake topologies in generic car models [22]. Regarding the development and trajectory of underbody vortex structures, our observations support the numerical findings of [13], which detailed the complex fluid dynamics governing underbody flow fields. Furthermore, the sensitivity of aerodynamic forces to variations in the diffuser configuration is consistent with the computational evaluations performed by [23] on wheeled vehicle geometries. However, as noted in comprehensive structural wake analyses such as those by [24], conventional fixed-angle diffusers are inherently limited by localized flow separations and lateral flow disturbances under shifting conditions. While these past studies underscore the global benefits of fixed expansions, the proposed variable-angle diffuser design in the present work introduces a dynamic mechanism to actively suppress side leakage and lateral

vortex intrusion. Consequently, this study expands the current literature by demonstrating that a variable geometric configuration can systematically overcome the aerodynamic compromises typical of static underbody devices.

Table 4 Output values and variances of C_D and C_L of the chosen models

Model	Drag Coeff. (C_D)	ΔC_D (counts)	Lift Coeff. (C_L)	ΔC_L (counts)
Base	0.2655	-	-0.005	-
wDiffuser	0.2170	485	-0.5045	499.5
wVariable Diffuser	0.2119	536	-0.4374	432.43

4. Conclusion

This study investigates the aerodynamic performance of a 35° Ahmed body equipped with fixed and variable underbody diffuser configurations. The analysis focused on drag behavior, wake structure, lateral vortex interaction and mass flow redistribution. Based on the numerical investigation carried out in this study, the following conclusions can be drawn:

- The fixed diffuser significantly increases the underbody mass flow and reduces the drag coefficient compared to the base configuration.
- Although the fixed diffuser improves drag performance, lateral vortex structures originating near the side edges interact with the diffuser exit and limit pressure recovery.
- The proposed variable diffuser modifies the expansion process and shifts the vortex core position away from the diffuser surface.
- The variable configuration provides an additional drag reduction of 51 drag counts compared to the fixed diffuser, reaching a total reduction of 536 drag counts relative to the base model.
- Mass flow analysis shows that the improvement is mainly related to changes in the underbody region, while the upper flow remains nearly unaffected.
- The reduction of side leakage results in a more stable wake structure and a smoother pressure distribution near the diffuser exit.

The results demonstrate that diffuser performance is influenced not only by expansion angle but also by its interaction with lateral vortex structures. In future work, different vehicle geometries and unsteady flow conditions can be considered to further evaluate the robustness of the proposed variable diffuser approach.

Nomenclature

Abbreviation/ Symbol	Description
C_D	Drag coefficient
C_L	Lift coefficient
L	Total length of the vehicle model [mm]
h	Height of the vehicle model [mm]
w	Width of the vehicle model [mm]
R_{eL}	Reynolds number based on vehicle length
U_∞	Free-stream inlet velocity [m/s]
x,y,z	Cartesian coordinates [m]
α	Rear slant angle [°]
θ	Diffuser expansion angle [°]
ΔC_D	Change in drag coefficient [counts]

Conflict of Interest Statement

The authors declare that they have no known competing financial interests or personal relationships that could have appeared to influence the work reported in this paper.

CRediT Authorship Contribution Statement

O. Baş: Conceptualization, Methodology, Software, Investigation, Formal Analysis, Visualization, Writing – Original Draft.
S. Keyinci: Conceptualization, Methodology, Validation, Supervision, Writing – Review & Editing, Final Approval.

5. References

1. Aultman, M., Duan, L., "Analysis of Flow Past a Double-Slanted Ahmed Body", Fluids, 10, 2, 35, 2025. doi: 10.3390/fluids10020035.
2. Liu, S., Chen, T., Zhou, W., "Numerical Analysis of Aerodynamic Drag Reduction for a DrivAer Automobile Model Using Rear Air Jets", Applied Sciences, 15, 22,

12334, 2025. doi: 10.3390/app152212334.
3. Akar, M.A., Baş, O., "Parametric, response surface, and adjoint optimizations of the underbody diffuser of a generic ground vehicle", International Journal for Numerical Methods in Fluids, 95, 9, 1468-1486, 2023. doi: 10.1002/fld.5198.
4. Connolly, M.G., Ivankovic, A., O'Rourke, M.J., "Drag reduction technology and devices for road vehicles - A comprehensive review", Heliyon, 10, 13, e33757, 2024. doi: 10.1016/j.heliyon.2024.e33757.
5. Ahmed, S.R., Ramm, G., Faltin, G., "Some salient features of the time-averaged ground vehicle wake", SAE Technical Paper, 840300, 1984. doi: 10.4271/840300.
6. Keiyinci, S., Baş, O., Akar, M.A., "Investigation on flow characteristics of generic car body with different boundary conditions", Scientia Iranica, 31, 13, 1077-1089, 2024. doi: 10.24200/sci.2023.59961.6523.
7. Viswanathan, H., "Aerodynamic performance of several passive vortex generator configurations on an Ahmed body subjected to yaw angles", Journal of the Brazilian Society of Mechanical Sciences and Engineering, 43, 3, 1-23, 2021. doi: 10.1007/s40430-021-02850-8.
8. Aguerre, H.J., Gimenez, J.M., Escribano, F., Nigro, N.M., "Aerodynamic study of a moving Ahmed body by numerical simulation", Journal of Wind Engineering and Industrial Aerodynamics, 245, 105635, 2024. doi: 10.1016/j.jweia.2023.105635.
9. Meile, W., Brenn, G., Reppenhagen, A., Lechner, B., Fuchs, A., "Experiments and numerical simulations on the aerodynamics of the Ahmed body", CFD Letters, 3, 1, 32-39, 2011.
10. Zhou, H., Chen, Q., Qin, R., Zhang, L., Li, H., "Investigation of wheelhouse shapes on the aerodynamic characteristics of a generic car model", Advances in Mechanical Engineering, 13, 12, 1-13, 2021. doi: 10.1177/16878140211066842.
11. Zhou, H., Qin, R., Wang, G., Xin, L., Wang, Q., Zheng, Z., "Comparative analysis of the aerodynamic behavior on Ahmed body mounted with different wheel configurations", Proceedings of the Institution of Mechanical Engineers, Part D: Journal of Automobile Engineering, 238, 1, 128-146, 2024. doi: 10.1177/09544070221121877.
12. Li, J., Zhang, Y., Zhou, R., Zhang, Z., Wang, G., "Investigation on aerodynamic force behavior and flow structure of Ahmed body under crosswind", Experimental Thermal and Fluid Science, 166, 111488, 2025. doi: 10.1016/j.expthermflusci.2025.111488.
13. Buscariolo, F.F., Assi, G.R.S., Sherwin, S.J., "Computational study on an Ahmed Body equipped with simplified underbody diffuser", Journal of Wind Engineering and Industrial Aerodynamics, 209, 104411, 2021. doi: 10.1016/j.jweia.2020.104411.
14. Guerrero, A., Castilla, R., Eid, G., "A Numerical Aerodynamic Analysis on the Effect of Rear Underbody Diffusers on Road Cars", Applied Sciences, 12, 8, 3763, 2022. doi: 10.3390/app12083763.
15. Huminic, A., Huminic, G., "Aerodynamics of curved underbody diffusers using CFD", Journal of Wind Engineering and Industrial Aerodynamics, 205, 104300, 2020. doi: 10.1016/j.jweia.2020.104300.
16. Ramana Murty Naidu, S.C.V., Madhavan, V.M., Chinta, S., Manikandan, R., Premkumar, A., Girimurugan, R., "Analysis of aerodynamic characteristics of car diffuser for dissimilar diffuser angles on Sedan's using CFD", Materials Today: Proceedings, 92, 240-248, 2023. doi: 10.1016/j.matpr.2023.04.379.
17. Jiang, F., Niu, J., Li, R., Wang, Y., Zhang, Y., "Computational Fluid Dynamics Analysis of Effect of Braking Plate Configurations on the Aerodynamic Behaviors of an Ahmed Car", Flow, Turbulence and Combustion, 110, 2, 301-323, 2023. doi: 10.1007/s10494-022-00388-w.
18. Keirsbulck, L., Cadot, O., Lippert, M., Boussemart, D., Basley, J., Delprat, S., et al., "Underbody flow control for base drag reduction of a real car model", Journal of Wind Engineering and Industrial Aerodynamics, 252, 105822, 2024. doi: 10.1016/j.jweia.2024.105822.
19. Porcar, L., Toet, W., Gamez-Montero, P.J., "Study of the effect of vertical airfoil endplates on diffusers in vehicle aerodynamics", Designs, 5, 3, 45, 2021. doi: 10.3390/designs5030045.

20. Polek, S., Chen, Y.T., Morris, M., “Flow over a 25° Ahmed body at a Reynolds number characteristic of suburban driving speeds”, International Journal of Heat and Fluid Flow, 106, 109318, 2024. doi: 10.1016/j.ijheatfluidflow.2024.109318.
21. Cheng, S.Y., Chin, K.Y., Mansor, S., Abd Rahman, A.B., “Experimental study of yaw angle effect on the aerodynamic characteristics of a road vehicle fitted with a rear spoiler”, Journal of Wind Engineering and Industrial Aerodynamics, 184, 305-312, 2019. doi: 10.1016/J.JWEIA.2018.11.033.
22. Huminic, A., Huminic, G., “Computational study of flow in the underbody diffuser for a simplified car model”, SAE Technical Paper, 2010-01-0119, 2010. doi: 10.4271/2010-01-0119.
23. Huminic, A., Huminic, G., “Aerodynamic study of a generic car model with wheels and underbody diffuser”, International Journal of Automotive Technology, 18, 3, 397-404, 2017. doi: 10.1007/s12239-017-0040-6.
24. Thacker, A., Aubrun, S., Leroy, A., Devinant, P., “Effects of suppressing the 3D separation on the rear slant on the flow structures around an Ahmed body”, Journal of Wind Engineering and Industrial Aerodynamics, 107-108, 237-243, 2012. doi: 10.1016/j.jweia.2012.04.022.